Heliyon 5 (2019) e02786

Contents lists available at ScienceDirect

Heliyon

journal homepage: www.heliyon.com

Research article

# Intercalation of water molecules from the air into perovskite and layered structures formed in the system of $NaNbO_3$–$Ca_2Nb_2O_7$

J.Y. Zubarev [a,*], Shun-Hsyung Chang [b], L.A. Shilkina [a], M.I. Mazuritskiy [c], A.P. Budnyk [d], A.V. Nazarenko [d], S.I. Dudkina [a], O.N. Razumovskaya [a], L.A. Reznichenko [a], I.A. Parinov [e]

[a] Scientific Research Institute of Physics, Southern Federal University, Stachki av. 194, 344090, Rostov-on-Don, Russia
[b] Department of Microelectronics Engineering, National Kaohsiung University of Science and Technology, Taiwan
[c] Department of Physics, Southern Federal University, Zorge st. 5b, 344090, Rostov-on-Don, Russia
[d] Federal Research Centre, The Southern Scientific Centre of the Russian Academy of Sciences, Chekhov Ave. 41, 344006, Rostov-on-Don, Russia
[e] Southern Federal University, Rostov-on-Don, Russia

ARTICLE INFO

*Keywords:*
Condensed matter physics
Materials science
Layered perovskite-like compounds
Ceramics
Calcium pyroniobate
Water intercalation

ABSTRACT

The study results of the perovskite solid solution and layered compounds formed in the system of (1-*x*)$NaNbO_3$-*x*$Ca_2Nb_2O_7$, $x = 0.10, 0.25, 0.55, 1.00$ are presented. The objects of the study are obtained by solid-phase synthesis, followed by sintering using conventional ceramic technology. The study of dielectric spectra has revealed their anomalous behavior in the temperature range of 360–450 K, most pronounced in the composition with $x = 0.25$. To explain the anomalies in these objects, a microstructural analysis of ceramics, thermogravimetry, high-temperature powder X-ray diffraction, and IR spectroscopy heve been performed. It has been established that the anomalies of the dielectric spectra in the indicated range are due to the adsorption of water from the air, its dissociation and the incorporation of the $OH_2$ and $OH^-$ oxyhydryl groups into the crystal lattice of the solid solution and the compounds. In a compound located near the boundary between solid solutions and layered compounds, the process of water adsorption is accompanied by the appearance of an intermediate incommensurate phase and ends with the formation of a new compound.

## 1. Introduction

The water-solid interaction is one of the most important issues in Materials Science. The water adsorption by materials with specific electrical and magnetic properties may lead to the formation of water-containing inclusions and hydrolysis products from the initial phases, worsening the properties of active materials [1].

Such materials include solid solutions (SS) and compounds formed in the binary system (1-*x*) $NaNbO_3$ – *x*$Ca_2Nb_2O_7$, where $0 \leq x \leq 1$. The interest to this system is piqued by the fact that its last components demonstrate some practically important properties. Sodium niobate is an antiferroelectric, and is used as a basis for environmentally friendly (lead-free) industrial piezoceramics. Calcium pyroniobate is a ferroelectric with a Curie temperature above 1800 K [2]. It is considered as a promising compound for non-linear optics [3] and laser technology [4]. In addition, $Ca_2Nb_2O_7$ is a highly active photocatalyst for water splitting under UV light irradiation [5, 6].

$NaNbO_3$ crystallizes in the perovskite-type structure with the general formula $ABO_3$. It has orthorhombic symmetry (space group Pbma) with the monoclinic perovskite subcell. The axial vectors of the orthorhombic cell A, B, C are related to those of the monoclinic subcell *a*, *b*, *c* as $\mathbf{A} = \boldsymbol{a}-\boldsymbol{c}$, $\mathbf{B} = 4\boldsymbol{b}$, $\mathbf{C} = \boldsymbol{a}+\boldsymbol{c}$, where $a = c = 3.915$ Å, $b = 3.885$ Å ($\beta = 90.64°$) [7]. $Ca_2Nb_2O_7$ possesses a perovskite-like layered structure (PLS) belonging to the homologous series of $A_nB_nO_{3n+2}$, with $n = 4$. There are two well-known modifications of $Ca_2Nb_2O_7$: one with monoclinic symmetry (space group P21) [8] and another one with orthorhombic symmetry (space group Cmcm) [9]. The orthorhombic calcium pyroniobate with cell parameters $a = 3.849$ Å, $b = 26.460$ Å, $c = 5.490$ Å has been synthesized for the present study.

The phase diagram for binary (1-*x*)$NaNbO_3$ – *x*$Ca_2Nb_2O_7$ consists of two fundamentally different concentration ranges [10]. In the $0.00 \leq x \leq 0.20$ range, the perovskite-type SS are formed on the basis of $NaNbO_3$, the symmetry of which changes from orthorhombic to cubic as the concentration of $Ca_2Nb_2O_7$ in the composition increases. In the $0.20 < x \leq 1.00$ region PLS of $A_nB_nO_{3n+2}$ ($n = 4$–10) series are formed.

Studying the dielectric properties of the described binary system,

* Corresponding author.
*E-mail address:* yzubarev@sfedu.ru (J.Y. Zubarev).

https://doi.org/10.1016/j.heliyon.2019.e02786
Received 20 February 2019; Received in revised form 23 May 2019; Accepted 1 November 2019

some anomalies in the temperature range of 360–450 K have been observed [11], which are presumedly due to the interaction of atmospheric water with ceramics. To prove the stated assumption the studies of four compositions corresponding to the different areas of the phase diagram have been performed in the present work. A plausible mechanism of water-solid interaction in PLS has been discussed.

## 2. Materials & methods

The objects of the present study are the composition of the binary system of (1-*x*)$NaNbO_3$ – *x*$Ca_2Nb_2O_7$ with $x = 0.10$ (NCN0.10), 0.25 (NCN0.25), 0.55 (NCN0.55), 1.00 (NCN1.00), characterizing different parts of the phase diagram (PD) system. The samples have been obtained by the method of solid-phase reaction, followed by sintering according to the usual ceramic technology. The initial reagents were $NaHCO_3$, $Nb_2O_5$ and $CaCO_3$ with the content of the main substance not lower than 99.9 %. The supplier of the raw materials is LLC "Rostekhnohim", Russia. The synthesis was performed in two stages with intermediate grinding of the samples. The temperature of the first synthesis was $T_1 = 1220$–$1250$ K, the temperature of the second synthesis was $T_2 = 1370$–$1470$ K (depending on composition), the time of the isothermal holding was $\tau_1 = \tau_2 = 4$ h. Sintering of the samples was performed at the following temperatures: NCN0.10 – $T_{sin} = 1560$ K, $\tau = 3$ h, NCN0.25 and NCN0.55 – $T_{sin} = 1620$ K, $\tau = 3$ and 2.5 h, respectively, NCN1.00 – $T_{sin} = 1650$ K, $\tau = 2.5$ h. In order to avoid losses of volatile components, the samples were baked during the synthesis and sintering in closed crucibles in the presence of the back filling (dispersed crystalline powder of the batch) of the same composition as the baked SS.

The experimental density of the ceramics was determined by the method of hydrostatic weighing in octane. X-ray density was calculated by the formula $\rho_{X\text{-ray}} = MZ/(N_A V)$, where $M$ is the molecular mass, $Z$ is the number of formula units per unit cell, $N_A$ is Avagadro's number, and $V$ is the unit cell volume. The relative density was found by the formula $\rho_{rel} = (\rho_{exp}/\rho_{X\text{-ray}})\cdot 100$. The relative densities of the manufactured ceramics NCN0.10 and NCN0.25 were 94 %, NCN0.55–78 %, NCN1.00–98 %.

After sintering, the samples were cut into disks with a diameter of about 1.0 cm and a thickness 0.10–0.15 cm. After the mechanical treatment, electrodes were deposited on the sample surface by twofold burning-in of a silver-containing paste at 1020 K for 0.5 h.

Micro X-ray fluorescence analysis (microXRFA) was performed on the M4 TORNADO microfluorescence spectrometer (Bruker) [12]. The source of the primary X-ray radiation was a low-power conventional X-ray tube (XRT) (30W) with a rhodium anode. It used the X-ray tube mode: U = 50kV, I = 300 μA. The microXRFA M4 TORNADO consisted of polycapillary lens (IFG Institute for Scientific Instruments [13]) used for focusing the primary radiation of the XRT into the spot diameter of 25 μm on a surface of the sample. Vacuum chamber of the micro-fluorescence spectrometer made it possible to do a quantitative analysis under pressure of 20 mbar and collect data for chemical elements beginning from 11Na. An energy dispersive detector with 4096 channels records and separates the energy of quanta with an energy resolution of 140 eV in the range of 1–40 keV. The use of M4 TORNADO at the "Multipoint" mode allowed us a statistically reliable collection of average intensities of X-ray fluorescence lines and to perform a quantitative analysis to determine the concentrations of the main chemical elements (11Na, 20Ca, 41Nb) contained in the studied ceramic samples.

The concentrations of chemical elements were determined by the method of fundamental parameters [14] using standard software of the spectrometer. Five areas with the size of 1 × 1.5 $mm^2$ were selected on the flat surface of each of the samples, each of which contained 100 points — uniformly distributed positions of the micro-focus of the polycapillary lens. Studies were performed with an exposure of 300 m s at each point. This corresponded to five local regions of the surface in which the intensities were measured and their averaged values were calculated. Thus, for each chemical element, the average values collected on the sample with a total volume of 500 measurements were used in calculating the concentrations.

The study of the microstructure of the samples was performed on a laser beam scanning microscope (LSM) KEYENCE VK-9700. The light source was a laser with a wavelength of 408 nm. Laser scanning resolution was 2048 × 1536 pixels with a 16-bit photomultiplier. The images of the internal structure on the cleaved samples with a magnification of 3000 times were obtained. The images were constructed using confocal microscopy. In that case, there was a sequential shooting of the images that were in focus at different heights. Everything that was above or below the focus was cut off by a confocal gap, and only the surface that was at a given height remained clear. Scanning was performed from top to bottom with a step of 0.1 μm (Z axis), after which all the images obtained at different heights were "stitched" to form a clear two-dimensional picture, and the data on the "height" (i.e., the vertical position of the eyepiece) made it possible to form a 3D visualization of the object under study without any contact with its surface.

High-temperature X-ray studies were performed by powder diffraction using an ADP-1 diffractometer (Bragg–Brentano focusing scheme, $Co_{K\alpha}$ - radiation). The samples for measurements were made in the form of a tablet pressed with polyvinyl alcohol from crushed ceramics, which was then glued to the sample holder with silicate glue with the addition of very small amounts of ZnO to improve the bond. The accuracy of the temperature stabilization in the chamber was ± 1K, the rate of the temperature rise was arbitrary. The parameters of the perovskite cell were calculated using the formulas corresponding to the monoclinic symmetry of the crystal lattice, simplified, and taking into account the small deviation of the perovskite cell from the cubic one [15].

$$d_{hkl} = \left(a \sin\beta \Big/ \sqrt{N}\right)\left(1 + k^2 y / N + lh \cos\beta / N\right), \quad (1)$$

where $N = h^2 + k^2 + l^2$, $h, k, l$ – diffraction indices, $y = b/(a\sin\beta) - 1$, $a, b, \alpha, \beta$ – perovskite cell parameters. Monoclinic cell parameters were calculated by the X-ray lines 200, 020, $20\bar{2}$. The measurement errors of the structural parameters had the following values: $\Delta a = \Delta b = \Delta c = \pm 0.004$ Å, $\Delta\beta = \pm 0.05^o$, $\Delta V = \pm 0.10$ $Å^3$. The parameters of the orthorhombic cell PLS were calculated using the corresponding quadratic form [16], along the lines 200, 0k0, 002. The measurement errors were: $\Delta a = \Delta c = \pm 0.007$ Å, $\Delta b = \pm 0.03$ Å, $\Delta V = \pm 2$ $Å^3$.

The Fourier-transform infrared (FTIR) measurements were performed on a Vertex 70 (Bruker) spectrometer. The powdered samples were mixed with KBr in a weight ratio of 1:100 and pressed into 1 mm thick tablets. The IR spectra were recorded in transmission mode with a 2 $cm^{-1}$ resolution in the 350–4000 cm-1 spectral range. The measured spectra (%T) were background-corrected and transformed into adsorbance values by using the instrument's software (Opus). The Diffuse Reflectance Ultra-Violet-Visible (DR-UV-Vis) spectra were obtained on a UV-2600 spectrophotometer (Shimadzu) using an integrating sphere accessory. The spectra were acquired with a 2 nm step in the two-beam geometry from a layer of the powdered samples against $BaSO_4$ as a reference. The measured spectra (in %R) were converted into the Kubelka-Munk function ($F$) values by using the instrument's software (UVProbe). The band gap ($E_g$) value was evaluated graphically for the indirect semiconductor from TAUC plot in the coordinates $(\alpha h\nu)^{1/2} = f(h\nu)$ and in $(\alpha h\nu)^2 = f(h\nu)$ for the direct one.

Thermogravimetric analysis (TGA) was performed on a STA 449 F5 Jupiter thermal analyzer (Netzsch). The powdered samples were treated in corundum crucibles at a heating rate of 10 K/min in the nitrogen atmosphere.

The dependences of the relative dielectric constant $\varepsilon/\varepsilon_0$ on temperature, at various frequencies ($f$) of the alternating electric field were determined using an Agilent E4285A precision LCR meter in the temperature range of 290–870 K and at 75 kHz–5 MHz frequencies. The study of the electrical conductivity was performed on a high resistance meter Agilent 4339B in the temperature range of 300–920 K. The

activation energy was determined from the dependences of the specific conductivity $\sigma$ on temperature by the formula:

$$W = k((\ln\sigma_1 - \ln\sigma_2) / (1 / T_1 - 1 / T_2)) \quad 2$$

where the coordinates $\sigma_1(T_1)$ и $\sigma_2(T_2)$ were selected from different parts of the rectilinear part of the graphs.

## 3. Results and discussion

### 3.1. XRF analysis

The micro-XRF analysis of the ceramic samples has shown that standard deviations for the average concentrations of the elements do not exceed 1% in correspondence to the values derived from their chemical formulas (see the Table.1). It confirms the specified ratios of cation concentration in the samples and preservation of composition stoichiometry, ensured by the chosen technology to produce solid solutions.

### 3.2. Microstructure

The LSM images of the cross-section area of the samples (after a long-term storage) are shown in Fig. 1. NCN0.10 consists of cubic-like crystallites of ~5 μm, while NCN0.25 is composed of lamellar grains in a wider size range of 7–20 μm, with individual plates extending up to 30 μm. Rod-shaped crystallites are likely to be the sides of lamellar grains. NCN0.55 possesses loose structure with lamellar large grains up to 15 μm and rod-like crystallites with sizes from 2 to 5 μm. Such morphology may be due to the presence of several phases in the sample. The structure of NCN1.00 is uniform, dense, the shape of the grains is lamellar and the grain size varies from 5 to 10 μm.

### 3.3. X-ray studies

The sample **NCN0.10** being a SS based on $NaNbO_3$, retains its structure, and has orthorhombic symmetry with a monoclinic perovskite cell. The parameters of the monoclinic cell are: $a = c = 3.906$ (2) Å, $b = 3.890$ (5) Å, $\beta = 90.62^o$. The XRD pattern of the sample is shown in Fig. 2a. In Fig. 2b the dependences of the parameters $a$, $b$, $\beta$ and the volume, $V$, of the monoclinic cell on temperature, and the change in the phase state of SS in the mode of heating and cooling are shown. At heating the following sequence of the phases change is established: $300 \leq T \leq 460$ K – $R(M_4)$ (*AFE P*) phase, $460 < T \leq 475$ K – $R(M_2)$ (*FE Q*) phase, $475 < T \leq 495$ K – pseudocubic phase ($Psc_2$), $T > 495$K cubic phase (*C*). Abbreviation P (M) means – orthorhombic symmetry with a monoclinic subcell. The low subscript indicates the degree of multiplication of the axis $b$ of the subcell. The areas of existence $Psc_2$ and $R(M_2)$ significantly expand during cooling. The transition of $Psc_2 \rightarrow R(M_2)$ occurs at 450 K, hysteresis is 25 K. The transition of $R(M_2) \rightarrow R(M_4)$ occurs at 345 K, hysteresis is 115 K. In the heating mode, two areas of anomalous behavior of the parameters and the cell volume are distinguished: $320 < T < 360$ K and $400 < T < 450$ K. In the first temperature range, there is a saltatory change in the linear parameters and the cell volume; in the second one, $a(T)$, $b(T)$, $V(T)$ have a wide minimum, while $\beta(T)$ has a very wide maximum.

At cooling $a(T)$ and $V(T)$ in *C* and *Psc* phases precisely repeat their course at heating; in the 400–450 K interval, all the dependences behave in the opposite way, and in the 320–360 K interval, there are no jumps in the parameters. It can be assumed that the jumps of $a$ and $V$ NCN0.10 in the region $320\text{K} < T < 360$ K during heating is caused by changes in the relative content of $P$ and $Q$ phases. The temperature ranges of the anomalous behavior of the dependences of the NCN0.10 structural parameters coincide with those in pure $NaNbO_3$ [17]. In this paper the following behavioral abnormalities of $NaNbO_3$ characteristics have been identified: $\varepsilon$ ($T$) (350 K, 420 K), a change in the slope of the temperature dependence of the relative elongation $\Delta L/L_0$ (430 K), the appearance of the incommensurate phase (410–460 K), the coexistence of the $P$ (AFE) and $Q$ (FE) phases (410–490 K), wherein the amount of $Q$ phase increases with increasing $T$ and decreases with cooling. In large $NaNbO_3$ single crystals [7], the $P$ and $Q$ phases coexist from room temperature to 530 K. It is noted that the appearance of the $Q$ phase in crystals is not reproducible and the conditions for its formation are not known. The parameter $a$ of the $Q$ phase cell is larger than the parameter $a$ of the $P$ phase (in $NaNbO_3$ by ≈ 0.006, 0.007 Å [7, 18]). Thus, the anomalies of the temperature dependences of all the parameters of the NCN0.10 SS, established in this study, are completely determined by the features of the $NaNbO_3$ structure. Another reason for the abnormal behavior of the structural characteristics of NCN0.10 may be the presence of oxyhydryl groups $O_mH_n$ in the SS structure. Depending on the degree and nature of the bond of the $O_mH_n$ groups with the crystal lattice, some leave the structure at $T < 370$ K, others – at $T > 370$ K [19]. The process of breaking the chemical bond and leaving the structure occurs in a certain temperature range and may be accompanied by the appearance of broad extremums on the temperature dependences of the structural characteristics.

The sample **NCN1.00** has orthorhombic symmetry with the cell parameters $a = 3.854$Å, $b = 26.47$ Å, $c = 5.502$ Å, $V = 561$ Å$^3$, the XRD pattern is shown in Fig. 3a. Fig. 3b shows the dependences of the parameters $a$, $b$, $c$, and $V$ of $Ca_2Nb_2O_7$ on temperature in the mode of heating and cooling. It can be seen that at heating, the monotonic behavior of $a$ ($T$), $b$ ($T$), $c$ ($T$) and $V$ ($T$) above 370 K is violated, and the fluctuations of the parameters and the cell volume do not exceed the measurement error. However, the jump of $b = -0.01$ Å at 370 K is not a random ejection, as confirmed by a gradual increase in $b$ with increasing temperature. In the same temperature range, the invar effect is observed in the dependences $a$ ($T$) and $c$ ($T$). At $T = 450$ K, a break is seen on all dependences, after which $a$ and $c$ practically do not change with increasing temperature, and the parameter $b$ behaves unstable. At cooling the sample, $a$ ($T$), $c$ ($T$) and $V$ ($T$) repeat their progress as during the heating process, except for the interval 390–370 K, where they all have a weakly pronounced maximum at 373 K. At cooling $b$ ($T$) there is no change in the slope; in the interval $523 > T > 440$ K, a decrease in $b$ occurs monotonously. The temperatures of the anomalies appearance indicate their possible connection with the water adsorption from the air, its decomposition and incorporation into the interlayer space of the NCN1.00 structure. This should lead to the increase in the cell parameter b, as it includes the width of the perovskite layer and the width of the interlayer space. If this assumption is correct, then at heating the sample in the region of 373 K, the desorption of water should occur and, as a result, a decrease in $b$, which is seen in Fig. 3 b.

The original sample **NCN0.25**, made in the form of ceramics in 2003, had the layered perovskite-like structure, the orthorhombic symmetry, the cell parameters at room temperature: $a = 5.512$ Å, $b = 60.07$ Å, $c =$

**Table 1**
Atomic concentrations (at.%) of the elements in the samples according to the chemical formula and to average concentrations measured by XRF.

| Sample | $NaNbO_3$ | | $0.9(NaNbO_3)+0.1(Ca_2Nb_2O_7)$ | | $0.75(NaNbO_3)+0.25(Ca_2Nb_2O_7)$ | | $0.45(NaNbO_3)+0.55(Ca_2Nb_2O_7)$ | | $Ca_2Nb_2O_7$ | |
|---|---|---|---|---|---|---|---|---|---|---|
| Element | Formula | XRF | Formula | XRF | Formula | XRF | Formula | XRF | Formula | XRF |
| $_{11}$**Na** | 50.0 | *50.3* | 40.9 | *40.4* | 30 | *29.8* | 14.5 | *15.1* | 0 | - |
| $_{20}$**Ca** | 0 | - | 9.1 | *10.1* | 20.0 | *19.4* | 35.5 | *34.7* | 50.0 | *50.7* |
| $_{41}$**Nb** | 50.0 | *49.7* | 50.0 | *49.5* | 50.0 | *50.8* | 50.0 | *50.2* | 50.0 | *49.2* |

Micro-XRF analysis data are shown in italics.

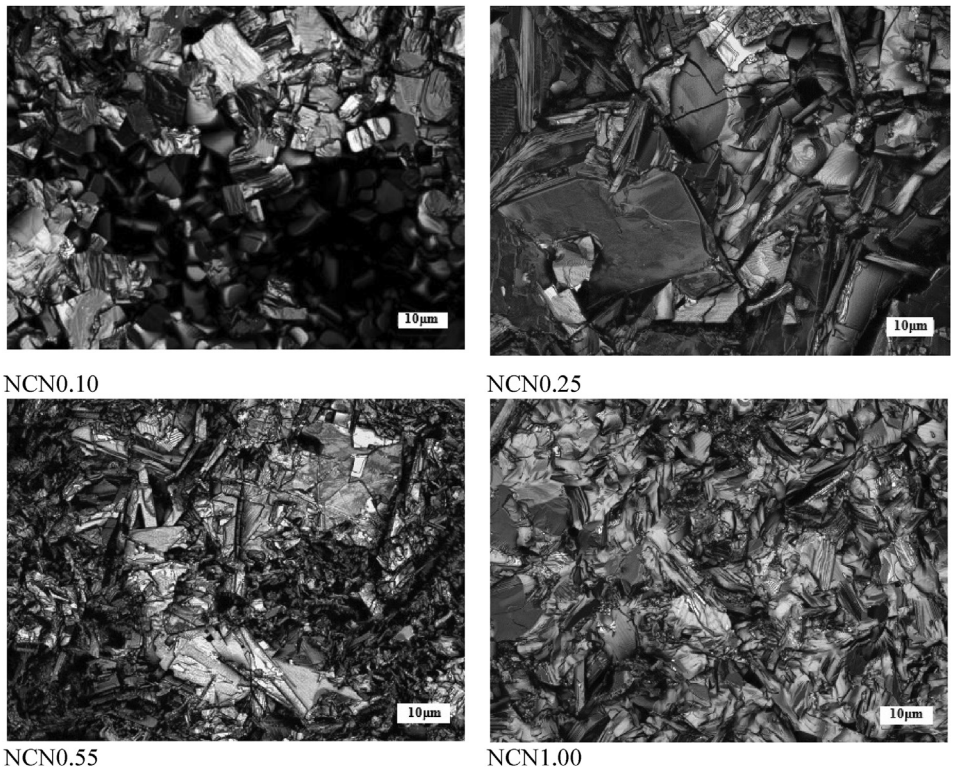


**Fig. 1.** LSM images of the cross-section area of the sintered samples.

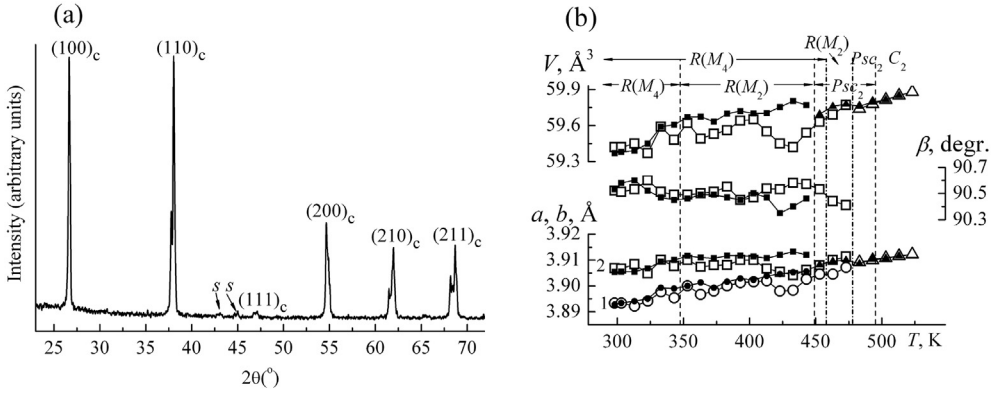


**Fig. 2.** (a) XRD pattern of the solid solution NCN0.10, indices (hkl) correspond to the pseudocubic perovskite cell, s - superstructural peaks. (b) Dependencies of the parameters $a = c$ (2), $b$ (1), β, volume, $V$, the monoclinic perovskite cell NCN0.10 on temperature in the heating (light icons) and cooling (black icons) modes. The circles and squares denote the parameters in the $R(M)$ phase, the triangles - in the *Psc* and *C* phases. Dashed lines indicate areas, which differ in the symmetry of the perovskite cell. The phase diagram at heating (above) and at cooling (below) is shown.

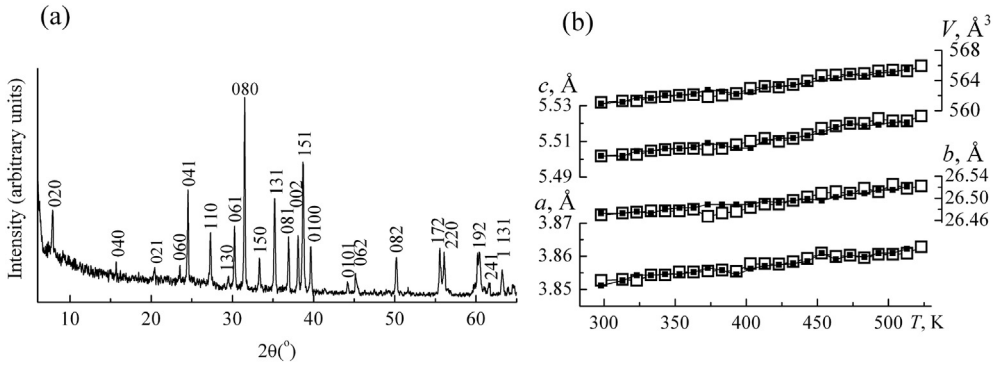


**Fig. 3.** (a) The XRD pattern of the initial sample NCN1.0, (b) Temperature dependences of parameters $a$, $b$, $c$ and volume, $V$, Ca2Nb2O7 cells in the heating (light icons) and cooling (black icons) modes.

3.898 Å, $V = 1290$ Å$^3$. The relationship between the perovskite $a_c$ (c – cubic symmetry) and orthorhombic cell parameters is: $a_n \approx \sqrt{2} \times a_c$, $b_n \approx n \cdot a_c\sqrt{2}+2K$, $c_n \approx a_c$ (K ≈ 2.25 Å - distance between layers) [20]. According to these relations, in the initial NCN0.25 $n = 10$ and the formula of the compound is $Na_6Ca_4Nb_{10}O_{32}$. After long-term storage, the layered structure and the orthorhombic symmetry of the sample are preserved, but the $b$ parameter has increased to 65.14 Å, while the $a$ and $c$ parameters have increased slightly. New cell parameters: $a = 5.518$ Å, $b = 65.14$ Å, $c = 3.903$ Å, $V = 1404$ Å$^3$, $n = 11$ and the compound formula is $Na_7Ca_4Nb_{11}O_{35}$. A similar effect was found by Chiba K. et al. [21] at studying *PLS* $Na_2Ca_2Nb_4O_{13}$ single crystals belonging to the Ruddlesden-Popper structure type. The authors observed an increase in the long parameter of the unit cell by 0.25 Å when the crystals were stored at ambient conditions for six months. The XRD patterns of the compounds of the original and after prolonged storage are presented in Fig. 4.

The peak marked on the XRD pattern 2 with the letter S could not be indexed in the selected cell, therefore we consider it as a satellite of the main line 200, $(110)_c$. The basis for this conclusion is that, in the group of the compounds $A_nB_nO_{3n+2}$, the alternation of dense perovskite layers with interlayer space occurs along the $[110]_c$ direction [22, 23] and can be accompanied by the modulation of the structure [24]. Therefore, the appearance of the strongest satellite near the peak 200 $(110)_c$ is quite likely. Calculated by the formula [16] $\Lambda = |1/d_{hkl} - 1/d_s|^{-1}$ ($d_{hkl}$, $d_s$ – are the interplanar distances of the main peak and the satellite, respectively) the modulation wavelength in the [100] direction of the orthorhombic cell $\Lambda = 59.8$ Å is a value close to the parameter $b$ of the original sample. The most likely cause of the increase in $b$ may be the water adsorption from the air, the dissociation of its molecules, and the intercalation of the oxygen into the layers with the formation of the additional layer of the oxygen octahedra. If our assumption is correct, then when this sample is heated above 373 K, its structure should return to its original state, since water adsorption is a reversible process [19]. In order to verify this, a study of NCN0.25 using powder X-ray diffraction in the temperature interval 293–523 K has been performed. The heating of NCN0.25 has been performed in two stages: first, the sample was heated to 423 K and then cooled to 343 K with the same step of 10 K and isothermal holding at each point for 10 min. The sample was cooled to room temperature with an oven. The next day, the sample was heated from 423 to 523 K in increments of 25 K, after that it was cooled with the oven to room temperature. At 293 K, the XRD pattern was recorded the next day (after 15 h) after heating, after 7 days, and after 21 days.

The study has shown that NCN0.25 (at room temperature, its condition was designated as the phase R1) above 373 K, through the intermediate phase (R2) returns to the state that corresponds to original NCN0.25 (phase R3). The symmetry of the intermediate phase R2 is also orthorhombic, and the cell parameter $b$ has an average value between the parameters $b$ of the phases R1 and R3, with almost the same parameters $a$ and $c$. Fig. 5a shows the XRD patterns of NCN0.25 in different phase states: at 293 K before heating (phase R1), 363 K (phases R1 + R2), 413 K (phases R2 + R3), 523 K (phase R3) and 293 K after heating (phases R3 and R1).

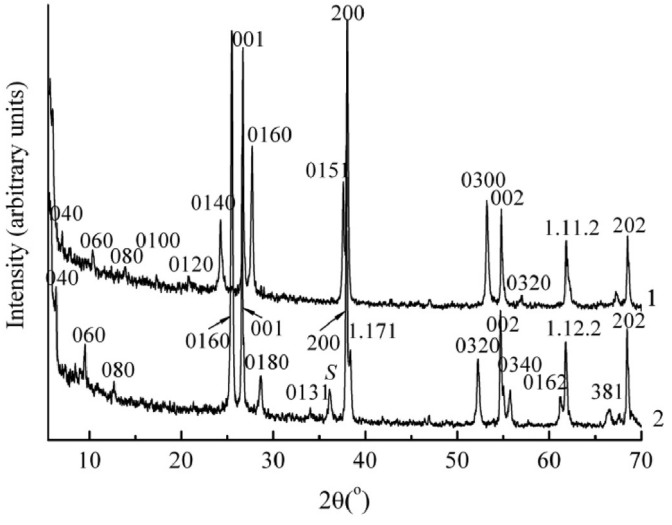


**Fig. 4.** The XRD patterns of the original sample NCN0.25 (1) and after long-term storage (2).

Fig. 5 b shows the fragments of the XRD patterns on an enlarged scale, illustrating the successive transition from the phase R1 to the phase R2 and then to the phase R3. It is clear that the phase R1 is maintained up to 353 K, at 363 K the peak of the phase R2 appears with the parameter $b = 61.83$ Å, the phases R1 and R2 coexist in the interval $353 < T < 383$ K. At 383 K, only the intermediate phase R2 remains, at 393 K, traces of the high-temperature phase R3 appear (Fig. 5 b). With the increase in temperature, the amount of the latter increases and above 448 K NCN0.25 completely passes into the R3 phase. At room temperature, 15 h after the measurements, two phases were present in NCN0.25 — high-temperature R3 and a small amount of the low-temperature phase R1 (Fig. 5 a). It should be noted that the intermediate phase R2 was absent at room temperature, regardless of the temperature from which the sample had been cooled, 423 K or 523 K, it was important that cooling occurred from the high-temperature phase R3. Seven days after the temperature measurements, NCN0.25 still remained two-phase – R1 + R3, but the R1 phase prevailed, and after 3 weeks the sample completely returned to the R1 phase.

In Fig. 6 the dependences of the parameters and the cell volume of the sample NCN0.25 on the temperature are shown. It can be seen that the parameter $b$ of the intermediate phase R2 in the wide range of its existence remains the same – 61.83 Å. At heating in the region of coexistence of the R1 and R2 phases, the parameters $a$ and $c$ and the cell volume of both phases also do not change – it is typical for the morphotropic phase transition in solid solutions [25, 26]. In the region of coexistence of R2 and R3 phases during heating, only parameters $a$ and $c$, which are the same in both phases, increase abruptly at 423 and 403 K, respectively. There are no other features on temperature dependencies. In the process of cooling, the dependences repeat the shape of the heating curves, but pass slightly lower than them till $T = 393$ K. At 383 K, all the parameters and volumes of the cell of the R2 and R3 phases increase, and are exceed their values at heating.

So, the results of the study allow us to make an unambiguous conclusion that the increase in the $b$ NCN0.25 parameter is due to the adsorption of the oxygen in the interlayer space. The adsorption-active centers in this case may be Na atoms located in the interlayer space and having a coordination number different from 12. This assumption has been made on the basis of data on the structure of $NaCa_4Nb_5O_{17}$ [23] and $Nd_4Ca_2Ti_6O_{20}$ [27], the compounds belonging to the $A_nB_nO_{3n+2}$ series. The authors of these works have found that A cations are located on the border of the perovskite layers, the number of which is greater in the compound. The appearance of the phase R2 with the parameter $b$, intermediate between the parameters $b$ of the phases R1 and R3, indicates that the adsorption of the oxygen in the interlayer space occurs similarly to the adsorption of atoms by the surface of mono- or polycrystalline objects. Due to lateral interaction, the adatoms are first adsorbed to one side of the interlayer space, with the result that the R2 phase appears with an intermediate parameter $b = 61.83$ Å, which corresponds to $n = 10.4$ [28]. In a certain temperature range, the low-temperature and intermediate phases coexist. When the adatoms fully occupy one side of the interlayer space, the other side begins to be filled up and the high-temperature phase R3 with $n = 11$ appears, coexisting with the intermediate phase in a certain temperature range. In our experiment, when the sample is heated, the oxygen desorption occurs first from one surface of the interlayer space, an intermediate phase appears, then the desorption from another surface and the transition of NCN0.25 to the initial state with $n = 10$. It is known [29] that during the

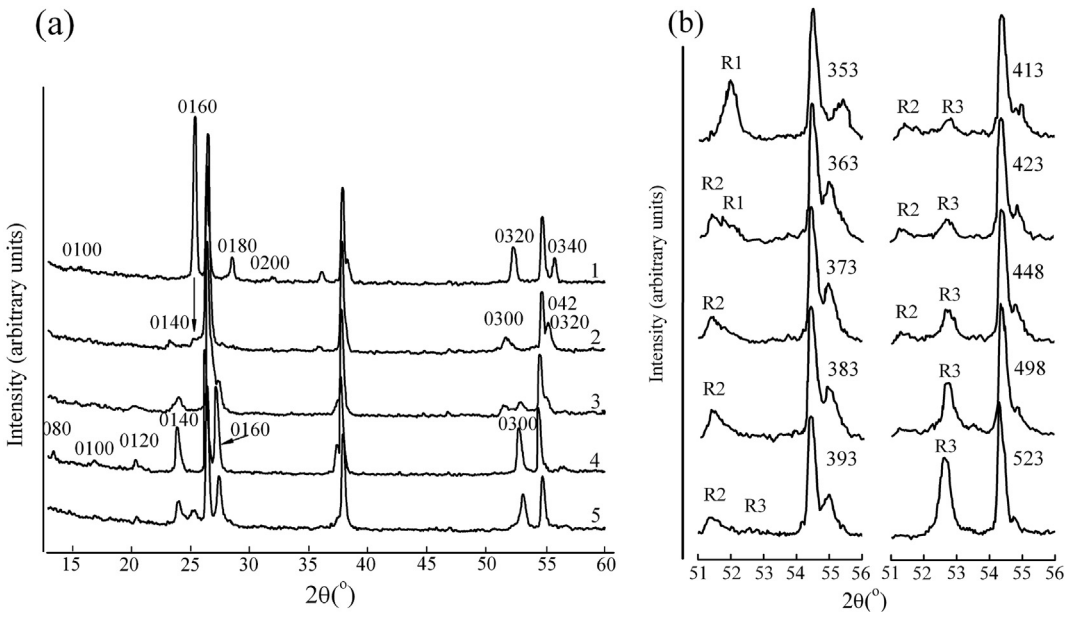


**Fig. 5.** (a) The XRD patterns of the sample NCN0.25 in the range of the angles 2θ 13-60° at different temperatures (cooling from 523 K), indexes are for diffraction reflections only 0*k*0: 1– 293 K before heating (phase R1), 2– 363 K (phase R2 and traces of the phase R1), 3– 413 K (phases R2 and R3), 4– 523 K (phase R3), 5– 293 K 15 h after the heating (phases R3 and R1), (b) Fragments of the XRD patterns of the sample NCN0.25 in the range of the angles 2θ 51-56°, and temperatures 353–, 523 K, illustrating the phase transition R1 → R2 → R3.

adsorption of the adatoms, the recovery of a sample occurs much faster if it is cooled from the temperature at which the intermediate phase exists. In order to ensure that the intermediate phase R2 appears as a result of oxygen adsorption, the sample NCN0.25 was heated to 383 K after its full recovery, where there was only intermediate phase R2, and then cooled to 303 K with the same step of 10° and a holding time of 10 min. At room temperature, the XRD patterns were recorded after 15 h and then 3 days after heating. The XRD patterns are shown in Fig. 7. It can be seen that after cooling NCN0.25 from 383 K after 15 h at room temperature, its radiograph does not contain the lines of the high-temperature phase; only the low-temperature phase R1 and a small amount of the intermediate phase R2 are present in the sample. After 3 days, NCN0.25 fully recovered to the R1 phase, while during cooling from the high-temperature R3 phase, the sample still remained biphasic in a week.

Thus, the study has shown that the layered compound $Na_6Ca_4Nb_{10}O_{32}$ formed in the binary system of $NaNbO_3$ – $Ca_2Nb_2O_7$ near

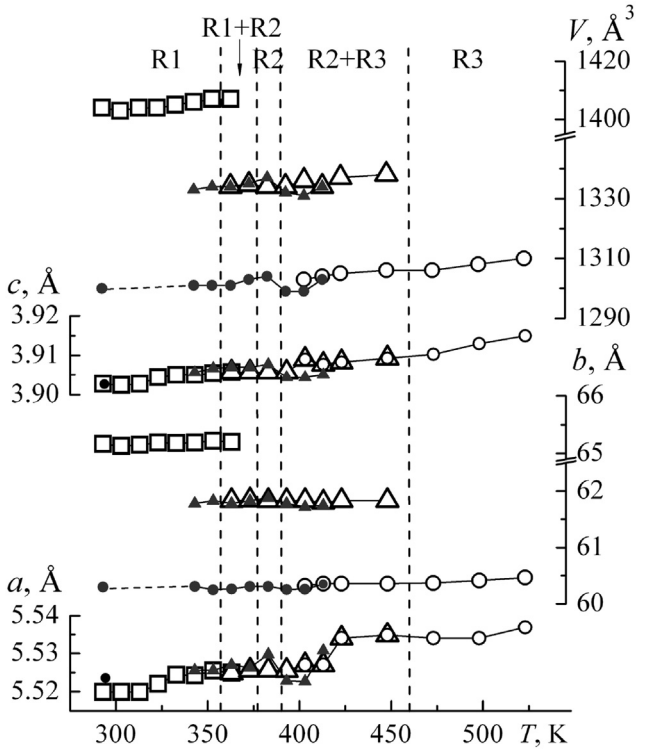


**Fig. 6.** Dependences of the parameters *a*, *b*, *c*, the volume, *V*, the orthorhombic cell of the sample NCN0.25 on temperature, dotted lines indicate areas differing in the phase composition during heating. The parameters and the volume of the phases are indicated by: R1 – squares, R2 – triangles, R3 – circles, light symbols – heating, black – cooling.

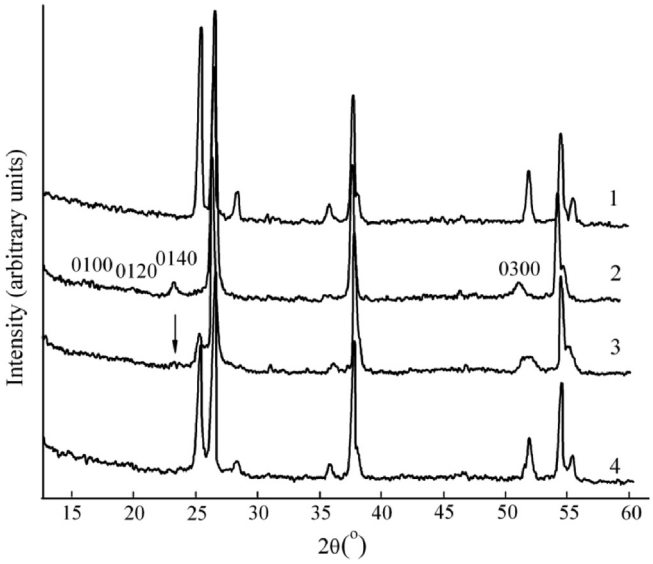


**Fig. 7.** The XRD patterns of the sample NCN0.25 in the range of the angles 2θ 13-60° (cooling from 383 K): 1– 293 K before heating (the phase R1), 2– 383 K (the phase R2), 3– 293 K after 15 h (the phase R1 and traces of the phase R2, are shown by the arrow), 4– 293 K 3 days after temperature measurements (the phase R1).

the border between solid solutions with the perovskite structure and PLS, has the ability to actively adsorb water from the air by dissociating it into the oxygen and the hydrogen. The oxygen is adsorbed into the interlayer space, being embedded in the crystal lattice, and as a result a new PLS is formed with greater $n$ – $Na_7Ca_4Nb_{11}O_{35}$, stable at room temperature.

The initial sample **NCN0.55,** right after its manufacture, consisted of two PLS with different thickness of the perovskite layer: $Na_2Ca_4Nb_6O_{20}$ ($n$ = 6) and $Na_4Ca_4Nb_8O_{26}$ ($n$ = 8) (Fig. 8). Both compounds had the pseudoorthorhombic symmetry, the cell parameters $Na_2Ca_4Nb_6O_{20}$: $a$ = 5.503 Å, $b$ = 37.79 Å, $c$ = 3.868 Å, $Na_4Ca_4Nb_8O_{26}$: $a$ = 5.502 Å, $b$ = 49.52 Å, $c$ = 3.896 Å. In Fig. 8 it can be seen that, after long-term storage, the phase composition of NCN0.55 did not change, but the amount of the compound with greater $n$ increased (on the XRD pattern (2), the intensity of its peaks 0k0 increased). The redistribution of the phases towards an increase in the concentration of the compound with a higher $n$ indicates the adsorption of water by the sample, its dissociation into the oxygen and the hydrogen and the incorporation of the oxygen into the crystal lattice of the layered compound with the formation of the additional layer of octahedra. In NCN0.55 this process occurs less intensively than in NCN0.25, because, as shown above with the latter example, the adsorption and structuring of the oxygen occurs more actively in the interlayer space containing $Na^+$ ions. The compounds that make up NCN0.55 in approximately equal amounts contain – one 2Na and 4Ca, the other – 4Na and 4Ca, while, in the original NCN0.25, the Na/Ca ratio is 6/4.

### 3.4. The IR spectroscopy

The FT-IR spectra of the samples are presented in Fig. 9. All of them contain a large band below 1000 $cm^{-1}$ due to the intrinsic adsorption of the material. It is asymmetric, with a maximum at 640 $cm^{-1}$ and a shoulder at 790 $cm^{-1}$. This vibrational envelope is formed by stretching vibrations of Nb–O bonds in $NbO_6$ polyhedra and will not be discussed in detail here. Instead, with the scope of our study, we will focus on the adsorption bands in the 3000–3700 $cm^{-1}$ interval and around 1630 $cm^{-1}$, where stretching and bending vibrations of adsorbed water molecules (and hydroxyl groups) are falling, respectively. These intervals are shown zoomed in the inset of Fig. 9. There are two bands centered at about 3440 and 3250 $cm^{-1}$ that can be distinguished in the higher-frequency interval by running a multiple peak fit with gaussians (shown by dashed curves in the inset of Fig. 9). The former band is larger and can be ascribed to weakly bonded water

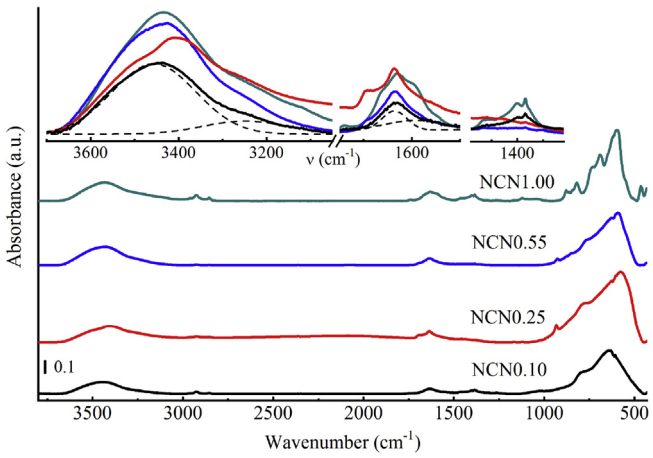


**Fig. 9.** FT-IR spectra of the samples. Spectra are shifted vertically for clarity. The inset shows an enlargement of spectral regions with vibrational signatures of adsorbed water molecules. The dashed curves are gaussians deconvoluting the spectral profile of NCN0.10.

molecules adsorbed on the surface. The lower-frequency band is consistent with that immanent to confined water (i.e. in the structure of ice), and can be attributed to water molecules embedded into the crystal lattice of the material through the formation of the weak hydrogen, weak ionic or partially covalent bonds [30]. The profile of NCN0.25 notably contains an additional component, situated at the intermediate position of ca. 3400 $cm^{-1}$. The attribution of this band is not straightforward; it might belong to intercalated water as well as to hydroxyl moieties from partially dissociated water molecules. In this regard, we recall that stretching vibrations of the O–H bonds in water molecules and those of the $OH^-$ groups are falling close (closely located), hence, the positions of the respective deformation vibrations are worth considering for their identification [19, 31]. Consequently, there are two components that can be individuated at 1635 and 1592 $cm^{-1}$ in the complex profile of the O–H bending band (inset in Fig. 9) for all the samples; with the additional shoulder at higher wavenumbers for NCN0.25 (at 1685 $cm^{-1}$) as well as for NCN1.00 (at 1655 $cm^{-1}$). The presence of three components in both vibrational intervals of NCN0.25 and NCN1.00 may be indicative for other types of water moieties being built differently into the structure of the compound.

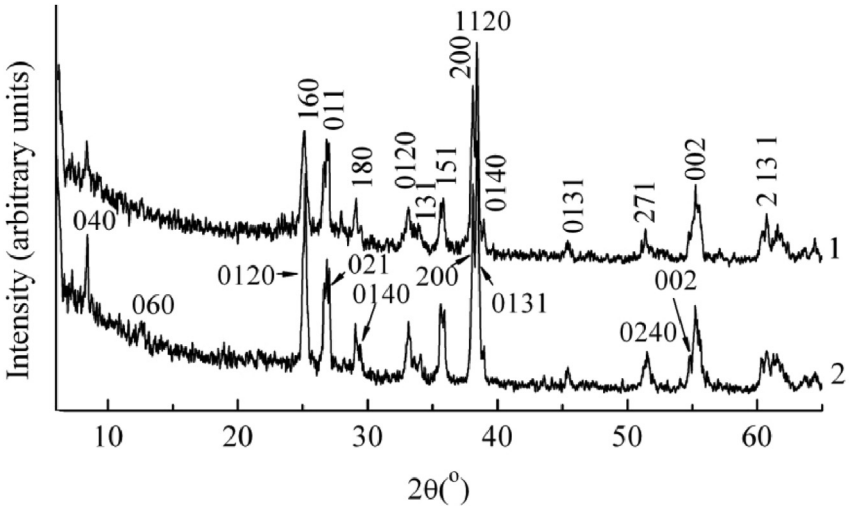


**Fig. 8.** The XRD patterns of the original (1) and after long-term storage (2) sample NCN0.55, which consists of the two PLS compound: $Na_2Ca_4Nb_6O_{20}$ and $Na_4Ca_4Nb_8O_{26}$, formed in the system (1-x) $NaNbO_3$–x$Ca_2Nb_2O_7$ at x = 0.55. On the the XRD pattern 1, the indexes of the diffraction reflections of only $Na_2Ca_4Nb_6O_{20}$ are shown, and on the XRD pattern 2, only the compounds of $Na_4Ca_4Nb_8O_{26}$ are shown.

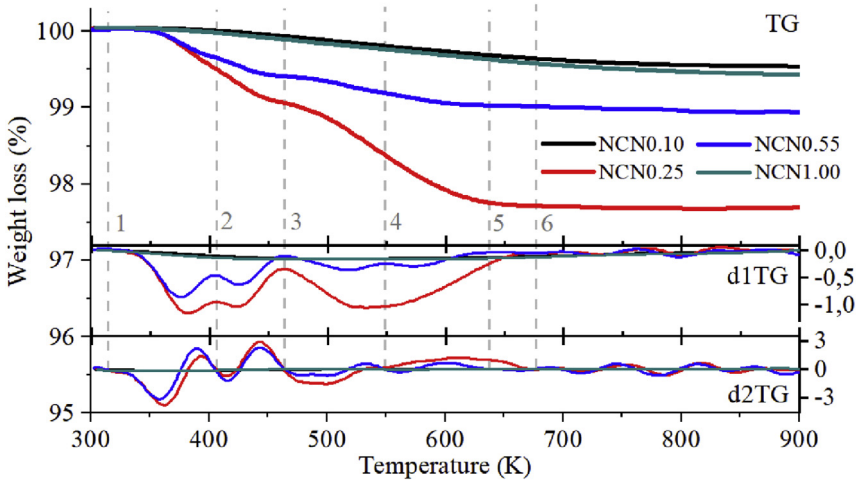


**Fig. 10.** The TGA curves of the samples under nitrogen (TG) and their first and second derivatives (d1TG and d2TG, respectively).

### 3.5. The TG analysis

The TGA curves were measured under nitrogen atmosphere for all the samples. Since the samples were sintered at much higher temperatures no structural changes were expected to occur in the course of the TGA measurement. The experimental curves are presented in Fig. 10 together with the first and second derivatives to facilitate the analysis. By the shape of the curves, the samples are divided into pairs of NCN0.10 and NCN1.00 showing the featureless curves with a modest overall weight loss of 0.5% and the other two with a distinct profile and a more noticeable final weight loss of 2.3% for NCN0.25 and of 1.1% for NCN0.55. Regarding the rigidity of the former pair we may presume that low amount of adsorbate (e.g. water molecules and hydroxide ions) is merely due to tightly packed dense grains of the samples. We also note here, that the samples are single compounds ($Ca_2Nb_2O_7$ as NCN1.00), or almost like them (NCN0.10).

The descent of the TG curves of the both NCN0.25 and NCN0.55 samples proceeded in several steps. Their limits were defined from the derivatives and marked with numbers (Fig. 10), allowing for the accurate evaluation of the step heights. The limit 1 at 313 K (40 °C) defines the beginning of the dehydration, which ends at 677 K (limit 5) for NCN0.25 and at 673 K (limit 6) for NCN0.55 (i.e. at ca. 400 °C for both). The three intermediate limits are located at 405, 464 and 548 K and separate four steps of weight loss. The first of them occurs at 382 K for NCN0.25 and at 374 K for NCN0.55, constituting 0.5 and 0.4%, respectively. The second one occurs at the same temperature of 423 K for the both samples, increasing the difference in weight loss from 0.1 to 0.4%. Next, NCN0.25 looses the rest 1.3% in one step at characteristic temperature of 537 K, while NCN0.55 proceeds in two steps of 517 and 573 K, decreasing for 0.4%. The final weight of NCN0.25 accounts for 97.7% of initial weight, while that of NCN0.55 is reduced to 98.9%. The overall weight loss for NCN0.55 is two times lower than that for NCN0.25 being in accordance to what had been observed with XRD and FT-IR techniques earlier.

There is no doubt, that in the first step, weakly physisorbed water is removed from the surface. According to the literature data [20], the following steps might correspond to the appearance and disappearance of the intermediate phase R2 in the form of water clusters. PLS NCN0.25 located on the phase diagram of the system near the boundary between the perovskite structure and layered phases, has the unique ability to adsorb water from the air. In $Na_6Ca_4Nb_{10}O_{32}$, water is absorbed, the oxygen is embedded in the lattice, and as a result a new layered compound appears with a larger thickness of the perovskite layer. Such chemical activity of the structure can lead to various anomalies of the physical properties of the compounds formed in the (1-$x$) $NaNbO_3$–$x$-$Ca_2Nb_2O_7$ system.

### 3.6. Dielectric studies

Fig. 11 shows the graphs of the dependences of the real part of the relative complex dielectric constant, $\varepsilon'/\varepsilon_0$, of the samples NCN0.10, NCN0.25, NCN0.55, and NCN1.00 at heating and at cooling. Fig. 12 presents the temperature dependences of the dielectric loss tangent, tg$\delta$.

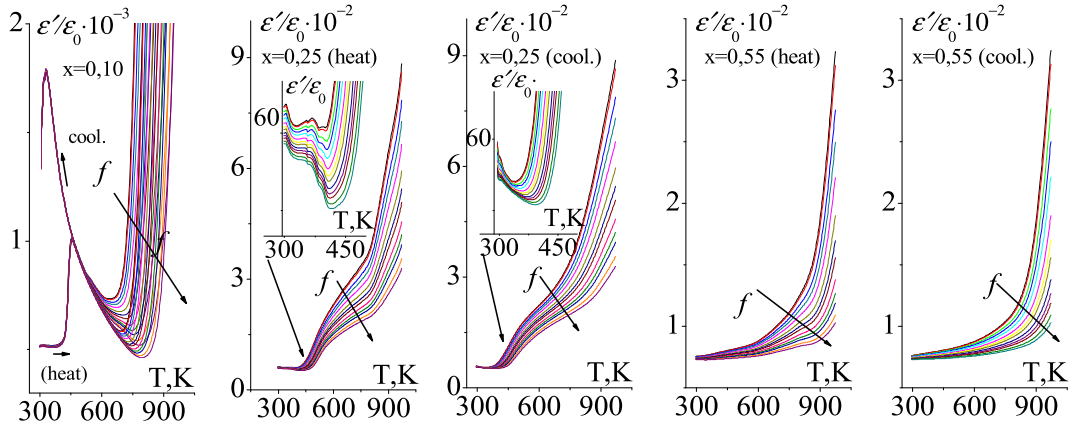


**Fig. 11.** Thermal frequency spectra of the real part of the relative dielectric constant, ε′/ε0, NCN0.10, NCN0.25, NCN0.55 during heating and cooling in the temperature range of 300–950 K and frequencies 75 kHz–5 MHz.

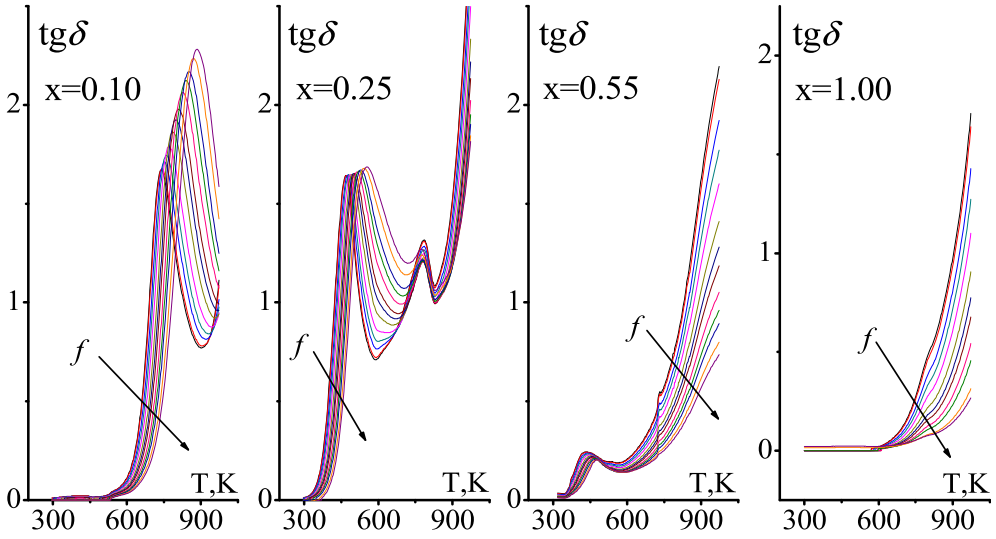


**Fig. 12.** The dependence of the dielectric loss tangent, tgδ, NCN0.10, NCN0.25, NCN0.55, and NCN1.00 on temperature.

It can be seen that the dispersion of the dielectric constant is absent in SS NCN0.10 in the temperature range of 300–500 K. The $\varepsilon'/\varepsilon_0(T)$ maximum of NCN0.10 at 470 K (Fig. 11) corresponds to the phase transition $R(M_4)\rightarrow R(M_2)$ (Fig. 2 b). In the cooling mode, the $\varepsilon'/\varepsilon_0$ maximum is shifted to the low temperature region by more than 100 K and corresponds to the $R(M_2)\rightarrow R(M_4)$ phase transition.

Structural changes in NCN0.25 in the dependences $\varepsilon'/\varepsilon_0(T)$ and $tg\delta(T)$ appeared by the increase in the dispersion with increasing temperature and by the maximum $tg\delta$ $(T)$ at 450 K, which corresponds to the phase transition R2 → R3. The features of the NCN0.25 structure are also reflected in the $\varepsilon'/\varepsilon_0(T)$ dependence in the heating – cooling mode. In the heating mode, the weak maximum $\varepsilon'/\varepsilon_0(T)$ in the region of 370 K, most noticeable at low frequencies, corresponds to the appearance of the intermediate phase R2 (see Fig. 6). Its absence in the cooling mode is due to the fact that when NCN0.25 is cooled from the high-temperature phase R3, the latter does not immediately go into the low-temperature phase R1, but remains at room temperature for several days (see Fig. 5 a).

In the NCN0.55 sample the weak $tg\delta(T)$ maximum (Fig. 12) at 450 K probably appears as a result of restructuring associated with the change in the quantitative ratio of the compounds, differing in the thickness of the perovskite layers. The appearance of the maximum in dielectric spectra, which disappears with increasing frequency of the electromagnetic field, and its absence during cooling, is probably due to the fact that water evaporates from the structure of the objects when heated, contributing to the overall picture.

In the heating-cooling mode at high temperatures, $T > 400$K, there are no significant differences in the character of the spectra. The dispersion in this area is most likely due to the reduction of niobium to the 4th valence state with the organization of the oxygen vacancies [32].

The ability of NCN0.25 to more actively capture water by a layered structure is confirmed by the low activation energy (Fig. 13). The nature of the dependences is determined by the contribution of the electronic conductivity due to the presence of the intrinsic defects (oxygen, sodium vacancies, and the adsorption products — desorption of trapped water).

If it is assumed that for the interval $T >$ 410–530 K the electrical conductivity is predominantly impure ionic, then a determining role of the same impurity in the conductivity of all SSs can be suggested.

It is noteworthy that the object NCN0.25 has the lowest activation energy (Fig. 13) of all, because of its greater reactivity (Hedvell effect) [33, 34] due to the "boundary" state on the PD system (between the perovskite and layered phases).

### 3.7. Optical spectra

DR-UV-Vis spectra of the samples are shown in Fig. 14a. There is a blue-shift of the fundamental adsorption edge with increasing $x$ in the (1-

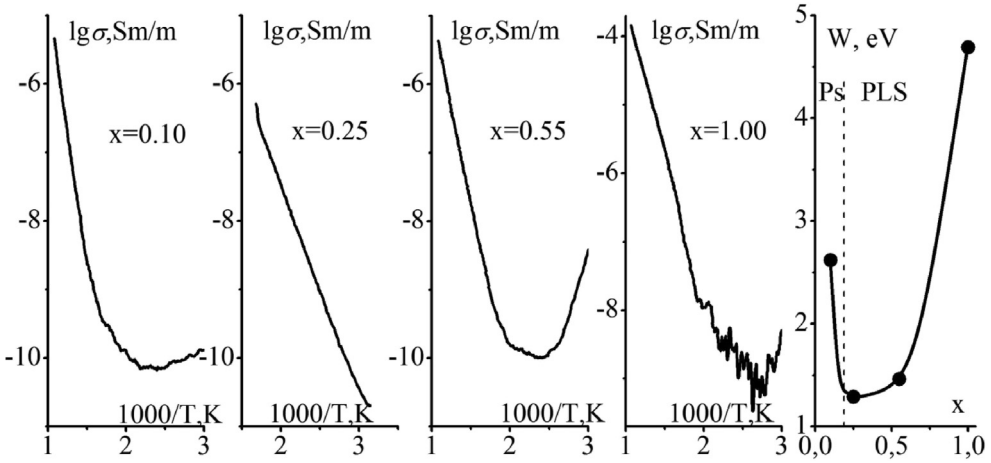


**Fig. 13.** The dependence of the logarithm of conductivity NCN0.10, NCN0.25, NCN0.55 and NCN1.00 on the inverse temperature. The dependence of the activation energy on $x$ (rightmost).

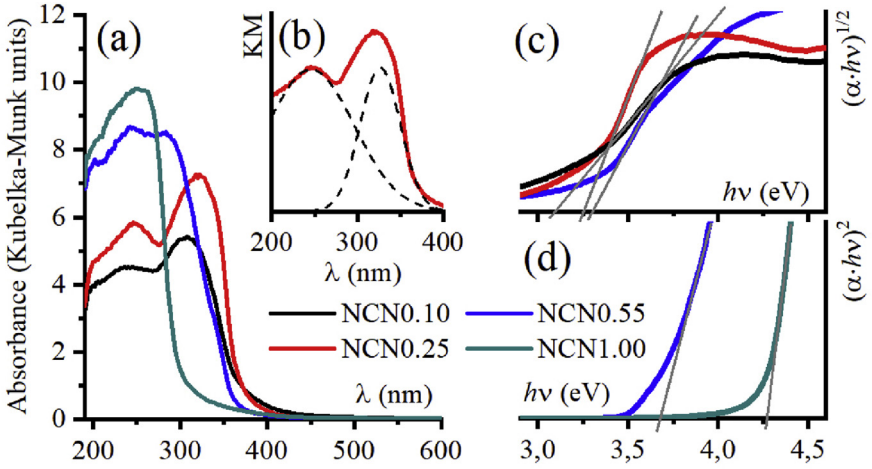


**Fig. 14.** (a) DR-UV-Vis spectra of the samples, (b) the example of fitting NCN0.25 with two gaussians, (c, d) the band gap energy analysis (TAUC plot).

$x$)$NaNbO_3$–$xCa_2Nb_2O_7$ composition, excluding NCN0.25, which once again confirms the mobility of its structure being in a certain reconstructive transition between two structural families. Looking at spectral profiles, it comes clear, that NCN1.00 ($Ca_2Nb_2O_7$) is characterized by the strong adsorption in the UV region, peaking at 252 nm. The introduction of $NaNbO_3$ to the composition leads to the formation of the second component at lower frequencies. The separation of two components is the most distinct for both NCN0.10 and NCN0.25. Fitting with gaussians (Fig. 14b) allows identifying two optical transitions bands at about 237 and 303 nm.

Taking into account that $NaNbO_3$ is considered as an indirect band-gap semiconductor, while $Ca_2Nb_2O_7$ is a direct band gap semiconductor. We have evaluated graphically the band gap of the samples from the primary optical transition (Fig. 14c,d). The obtained values are 3.11 and 3.26 eV for NCN0.10 and NCN0.25, respectively. Since NCN0.55 contains both compounds in nearly equal proportions, its TAUC plot curve has two linear sections (Fig. 14c). These intervals have been approached separately, giving 3.28 eV (the evaluation as the indirect band gap semiconductor, Fig. 14c) and 3.68 eV (as the direct band gap material, Fig. 14d). The band gap of NCN1.00 has been found to be 4.28 eV (Fig. 14d). The obtained values comply well with known optical properties of both $NaNbO_3$ and $Ca_2Nb_2O_7$. Large values of the band gap make the direct use of these materials as photocatalysts under visible light less likely, although, both NCN0.10 and NCN0.25 appear to be promising in this regard, and worth of further studies.

## 4. Conclusions

In the present work, it has been shown that the layered compound of the homologous $A_nB_nO_{3n+2}$ series is formed in the (1–$x$)$NaNbO_3$–$xCa_2Nb_2O_7$ system near the boundary between the perovskite structure and layered phases. This compound has the unique ability to adsorb water from the air, which then decomposes into the oxygen and the hydrogen. The oxygen is embedded in the interlayer space PLS forming a layered compound with a greater thickness of the perovskite layer. The hydrogen evaporates, and its output is much greater than during adsorption and decomposition of water by the compound $Ca_2Nb_2O_7$. The restoration of the original structure of the compound $Na_6Ca_4Nb_{10}O_{32}$ after the desorption of water occurs at different rates, depending on the stage of the desorption at which cooling occurs.

The complete correlation of the structural changes and anomalies of the dielectric properties of the solid solution with $x = 0.10$, and the compounds formed in the system at $x = 0.25$ and 0.55, is established.

## Declarations

### *Author contribution statement*

J.Y. Zubarev, L.A. Shilkina, M.I. Mazuritskiy, A.P. Budnyk, A.V. Nazarenko, S.I. Dudkina: Performed the experiments; Wrote the paper.

Shun-Hsyung Chang, I.A. Parinov: Analyzed and interpreted the data.

O.N. Razumovskaya: Contributed reagents, materials, analysis tools or data.

L.A. Reznichenko: Conceived and designed the experiments.

### *Funding statement*

This work was supported by the state task of the Ministry of Education and Science of the Russian Federation (3.6371.2017/8.9, 3.6439.2017/8.9 and №– 16.3871.2017/4.6) within the framework of the SSC RAS State Order for 2018 (01201354247) and the Russian Foundation for Basic Research in the framework of a scientific project (17-08-01724, 19-08-00365_a); MOST107-2221-E-992-027, MOST108-2221-E992-026.

### *Competing interest statement*

The authors declare no conflict of interest.

### *Additional information*

No additional information is available for this paper.

## Acknowledgements

We would like to thank the Center for Collective Use: "Electromagnetic, Electromechanical and Thermal Properties of Solids" of Research Institute of Physics, Southern Federal University.

## References

[1] M.A. Henderson, The interaction of water with solid surfaces: fundamental aspects revisited, Surf. Sci. Rep. 46 (1-8) (2002) 1–308.

[2] H. Ning, H. Yan, M.J. Reece, Piezoelectric stronrium niobate and calcium niobate ceramics with super-high Curie points, J. Am. Ceram. Soc. 93 (2010) 1409–1413.

[3] X. Long, X. Han, Growth of nonlinear optical calcium pyroniobate crystal, J. Cryst. Growth. 275 (3-4) (2005) 492–495.

[4] C. Wu, Y. Li, H. Gong, J. Gao, Z. Wang, Niobium-oxygen octahedra and oxygen interstitial defect emissions in calcium niobate matrix and its color manipulation via doping Pr3+, AIP Adv. 7 (2017), 025019-1-6.

[5] H.G. Kim, D.W. Hwang, J. Kim, Y.G. Kim, J.S. Lee, Highly donor-doped (110) layered perovskite materials as novel photocatalysts for overall water splitting, Chem. Commun. (1999) 1077–1078.

[6] A. Nakamura, O. Tomita, M. Higashi, S. Hosokawa, T. Tanaka, R. Abe, Solvothermal synthesis of $Ca_2Nb_2O_7$ fine particles and their high activity for photocatalytic water splitting into $H_2$ and $O_2$ under UV light irradiation, Chem. Lett. 44 (3) (2015) 1001–1003.

[7] A.M. Glazer, H.D. Megaw, Studies of the lattice parameters and domains in the phase transitions of $NaNbO_3$, Acta Cryst. A. 29 (1973) 489–494.

[8] S. Nanamatsu, M. Kimura, Ferroelectric properties of $Ca_2Nb_2O_7$ single crystal, J. Phys. Soc. Japan. 36 (1974) 1495.

[9] L.H. Brixner, K. Babcock, Inorganic single crystals from reactions in fused salts, Mater. Res. Bull. 3 (1968) 817–824.

[10] J.Y. Zubarev, L.A. Shilkina, L.A. Reznichenko, Phase state patterns and dielectric properties of solid solutions of binary systems (1-*x*)$NaNbO_3$–*x*$Sr_2Nb_2O_7$, (1-*x*) $NaNbO_3$-*x*$Ca_2Nb_2O_7$, Bull. RAS: Phys 80 (11) (2016) 1536–1538.

[11] J.Y. Zubarev, I.A. Verbenko, L.A. Reznichenko, O.N. Razumovskaya, Anomalies in the dielectric properties of compounds and solid solutions of a binary system (1-x) NaNbO3 – xCa2Nb2O7 with $0.00 \leq x \leq 1.00$ in the range 300–450 K: «water dance», in: Abst. And Schedule Book 2017 International Conference on "Physics and Mechanics of New Materials and Their Applications" (PHENMA 2017), Jabalpur, India, October 14-16, 2017, pp. 312–313.

[12] Bruker Corporation 2D X-ray Fluorescence (Micro-XRF) M4 Tornado (https://www.bruker.com/products/x-ray-diffraction-and-elemental-analysis/micro-xrf-and-txrf/m4-tornado/overview.html.

[13] IfG – Institute for Scientific Instruments GmbH, Rudower Chaussee 29/31 12489 Berlin, Germany (http://www.ifg-adlershof.de).

[14] B. Beckhoff, B. Kanngieber, N. Langhoff, et al., Hand Book of Practical X-Ray Fluorescence Analysis, Springer, 2006.

[15] E.G. Fesenko, Perovskite Family and Ferroelectricity, Atomizdat, Moscow, 1972.

[16] A. Guinier, Theorie et Technique de la Radiocristallographie, Pris Dunod, 1956.

[17] L.A. Reznichenko, L.A. Shilkina, E.S. Gagarina, I.P. Raevsky, E.I. Dulkin, E.M. Kuznetsova, V.V. Akhnazarova, Structural instabilities, disproportionate modulations, P- and Q-phases in sodium niobate in the range of 300–500 K, Crystallography. 48 (3) (2003) 493–501.

[18] I. Lefkowitz, K. Lukaszewicz, H.D. Megaw, The high-temperature phases of sodium niobate and the nature of transitions in psevdosymmetric structures, Acta Cryst. 20 (1966) 670–683.

[19] G.V. Yuhnevich, Infrared Water Spectroscopy, Nauka, Moscow, 1973.

[20] M. Nanot, F. Queyroux, J.-C. Gilles, A. Carpy, J. Galy, Phases multiples dans les Systemes $Ca_2Nb_2O_7$-$NaNbO_3$: les series homologues de formule $A_nB_nO_{3n+2}$, J. Solid State Chem. 11 (1974) 272–284.

[21] K. Chiba, N. Ishizawa, S. Oishi, A Ruddlesden-Popper-type layered perovskite, $Na_2Ca_2Nb_4O_{13}$, Acta Cryst. C. 55 (1999) 1041–1044.

[22] I. Levin, L.A. Bendersky, Symmetry classification of the layered perovskite-derived $A_nB_nX_{3n+2}$ structures, Acta Cryst. B Structural Science Crystal Engineering Materials 55 (6) (1999) 853–866.

[23] F.J. Zuniga, J. Darriet, $NaCa_4Nb_5O_{17}$: a layered perovskite $A_nB_nO_{3n+2}$ compound, Acta Cryst. C. 59 (2003) i18–i20.

[24] N.B. Bolotina, X-ray analysis of modulated crystals, Overview, Crystallography 52 (4) (2007) 673–685.

[25] I.N. Andryushina, L.A. Reznichenko, L.A. Shilkina, K.P. Andryushin, S.I. Dudkina, The PZT system ($PbTi_xZr_{1-x}O_3$, $0 \leq x \leq 1.0$): the real phase diagram of solid solutions (Room temperature) (Part 2), Ceram. Int. 39 (2) (2013) 1285–1292.

[26] I.N. Andryushina, L.A. Reznichenko, L.A. Shilkina, K.P. Andryushin, S.I. Dudkina, The PZT system ($PbTi_xZr_{1-x}O_3$, $0 \leq x \leq 1.0$): high temperature x-ray diffraction studies. Complete *x*-T phase diagram of real solid solutions (Part 3), Ceram. Int. 39 (3) (2013) 2889–2901.

[27] R. Portie, A. Carpy, M. Fayard, J. Galy, Perovskite-like compounds $ABO_{3+x}$ ($0.44 \leq x < 0.5$). Electron microscopy survey on the $(NaCa)_nNb_nO_{3n+2}$ ($4 < n \leq 4.5$) homologous series, Phys. Stat. Sol. (a) 30 (1975) 683–697.

[28] B.V. Andryushechkin, A.M. Prokhorov, The current state of studies of structural phase transitions in adsorbed layers, Proc. of the Inst. of Gen. Phys. 66 (2010) 6–19.

[29] O. M Brown, V.K. Medvedev, The interaction between particles adsorbed on the surface of metals, UFN. 157 (4) (1989) 631–666.

[30] K. Nakamoto, IR Spectra and Raman Spectra of Inorganic and Coordination Compounds, Mir, Moscow, 1991.

[31] B.N. Tarasevich, IR Spectra of the Main Classes of Organic compounds. Reference Materials, Pub. House of MSU, Moscow, 2012.

[32] G.C. Vezzoli, Electrical properties of $NbO_2$ and $Nb_2O_5$ at elevated temperature in air and flowing argon, Phys.Rev.B 26 (7) (1982) 3954–3957.

[33] K. Meyer, Physikalisch-chemische Kristallographie, VEB Deutscher Verlag fur Grundstoffindusrie, Leipzig, 1968.

[34] I.Z. Hedvell, Phys. Chem. (1926) 331250331.